Measurement of RyR permeability reveals a role of calsequestrin in termination of SR Ca^{2+} release in skeletal muscle

Monika Sztretye,[1] Jianxun Yi,[1] Lourdes Figueroa,[1] Jingsong Zhou,[1] Leandro Royer,[1] Paul Allen,[2] Gustavo Brum,[3] and Eduardo Ríos[1]

[1]Section of Cellular Signaling, Department of Molecular Biophysics and Physiology, Rush University, Chicago, IL 60612
[2]Department of Anesthesia, Perioperative, and Pain Medicine, Brigham and Women's Hospital, Harvard Medical School, Boston, MA 02115
[3]Departamento de Biofísica, Facultad de Medicina, Universidad de la República, 11800 Montevideo, Uruguay

The mechanisms that terminate Ca^{2+} release from the sarcoplasmic reticulum are not fully understood. D4cpv-Casq1 (Sztretye et al. 2011. *J. Gen. Physiol.* doi:10.1085/jgp.201010591) was used in mouse skeletal muscle cells under voltage clamp to measure free Ca^{2+} concentration inside the sarcoplasmic reticulum (SR), [Ca^{2+}]$_{SR}$, simultaneously with that in the cytosol, [Ca^{2+}]$_c$, during the response to long-lasting depolarization of the plasma membrane. The ratio of Ca^{2+} release flux (derived from [Ca^{2+}]$_c(t)$) over the gradient that drives it (essentially equal to [Ca^{2+}]$_{SR}$) provided directly, for the first time, a dynamic measure of the permeability to Ca^{2+} of the releasing SR membrane. During maximal depolarization, flux rapidly rises to a peak and then decays. Before 0.5 s, [Ca^{2+}]$_{SR}$ stabilized at ∼35% of its resting level; depletion was therefore incomplete. By 0.4 s of depolarization, the measured permeability decayed to ∼10% of maximum, indicating ryanodine receptor channel closure. Inactivation of the t tubule voltage sensor was immeasurably small by this time and thus not a significant factor in channel closure. In cells of mice null for Casq1, permeability did not decrease in the same way, indicating that calsequestrin (Casq) is essential in the mechanism of channel closure and termination of Ca^{2+} release. The absence of this mechanism explains why the total amount of calcium releasable by depolarization is not greatly reduced in Casq-null muscle (Royer et al. 2010. *J. Gen. Physiol.* doi:10.1085/jgp.201010454). When the fast buffer BAPTA was introduced in the cytosol, release flux became more intense, and the SR emptied earlier. The consequent reduction in permeability accelerated as well, reaching comparable decay at earlier times but comparable levels of depletion. This observation indicates that [Ca^{2+}]$_{SR}$, sensed by Casq and transmitted to the channels presumably via connecting proteins, is determinant to cause the closure that terminates Ca^{2+} release.

INTRODUCTION

The intracellular signal for contraction of skeletal muscle is the rapid increase in free cytosolic [Ca^{2+}]. This increase requires coordinated opening of a substantial fraction of intracellular Ca^{2+} release channels of the SR, which allows for a large flux of Ca^{2+} from stores to cytosol. This flux must terminate rapidly as well to allow for the fast decay of [Ca^{2+}] required for mechanical relaxation.

The mechanisms that terminate Ca^{2+} release flux may include both a reduction in the openness of the release channels and a reduction in the current per channel, as the SR depletes and the driving force for Ca^{2+} flux is reduced. The relative contribution of such gating and depletion processes is not known quantitatively for skeletal muscle. In cardiac muscle, where more is known, an interaction has been demonstrated whereby depletion reduces flux both directly, by reducing the [Ca^{2+}] gradient,

and indirectly, through an effect on channel gating (e.g., Györke and Terentyev, 2008). The depletion–gating interaction appears to require the presence of proteins of the junctional complex, calsequestrin (Casq), and its junction-anchoring proteins triadin and junctin.

One of the difficulties found in defining these mechanisms in skeletal muscle is the lack of reliable methods to accurately monitor free intra-SR [Ca^{2+}], [Ca^{2+}]$_{SR}$, which is required for the identification of changes in driving gradients and their separation from changes in channel openness.

The companion paper in this issue (Sztretye et al.) validated a novel method to monitor [Ca^{2+}]$_{SR}$. In this study, we report results obtained with this method, which was applied to living cells in parallel with conventional measurements of cytosolic Ca transients. The flux of Ca release, $\dot{Rel}(t)$, was derived from the measured transients of [Ca^{2+}]$_c$ and combined with the measured

The Rockefeller University Press $30.00
J. Gen. Physiol. Vol. 138 No. 2 231–247
www.jgp.org/cgi/doi/10.1085/jgp.201010592

231

$[Ca^{2+}]_{SR}$ for a direct calculation of permeability of the release pathway, a variable which has not been evaluated directly until now.

Such direct measurement allowed us to observe that prolonged Ca^{2+} release results in major depletion of SR content, sharply reducing free $[Ca^{2+}]_{SR}$. This is accompanied by a reduction in SR permeability during Ca^{2+} release. To test the hypothesis that the change in permeability is determined by the reduction in $[Ca^{2+}]_{SR}$, we substituted a fast exogenous buffer, BAPTA, for the conventionally used EGTA, which drastically changed the speed of depletion and the timing of the decrease in SR permeability. To determine whether the changes in permeability require the presence of Casq as previously suggested for cardiac muscle, the measurements were repeated in muscles of mice null for the skeletal muscle isoform of Casq.

MATERIALS AND METHODS

The methods used in the present study were largely described in the companion paper (Sztretye et al., 2011). In this study, described in addition are simultaneous imaging using the monitor of $[Ca^{2+}]_{SR}$, D4cpv (Palmer et al., 2006) fused to Casq1 or its δAsp variant, and the high affinity indicator X-rhod-1 (Invitrogen) placed in the cytosol by diffusion from a patch pipette.

All experiments described here were performed on cells under voltage clamp. The intramembranous charge displacement Q_n (V_m), integral over time of the charge movement current I_Q, reflecting the responses of the transverse tubule voltage sensor, was measured as described in the companion paper (Sztretye et al., 2011). Its Boltzmann parameters were not different than in earlier work (Royer et al., 2008, 2010), with the exception of the group of cells studied with BAPTA in the internal solution, which had a transition voltage, V_T, shifted by ∼11 mV in the positive direction. All dynamic responses shown in this paper were obtained with depolarizing pulses to 30 mV, thus ensuring essentially full activation, regardless of the shift in transition voltage. The pulses were of a duration well in excess of that needed to reach a steady level of cytosolic Ca concentration ($[Ca^{2+}]_c$), namely 400–500 ms in experiments using BAPTA or 1–1.5 s in experiments with EGTA.

In a separate series of experiments, we investigated whether a depolarization to 30 mV lasting 400 ms could cause inactivation of the t tubule voltage sensor. In these experiments (see Fig. 6), Q_n was measured during brief depolarizations to voltages V_m, and the effects therein of a preceding conditioning depolarization (of 400 ms to 30 mV; see Fig. 6 A) were evaluated.

Compositions of solutions "External," "BAPTA," "EGTA," and "Depletion Cocktail" are given in the companion paper (Sztretye et al., 2011). All experiments were performed at room temperature (20–22°C).

Confocal scanning and determination of $[Ca^{2+}]_{SR}$

Images F_1 and F_2 of fluorescence of D4cpv-Casq1 and D4cpv-δAsp and F_3 of X-rhod-1 were acquired in a laser-scanning confocal system equipped with acousto-optical tunable filters and dichroic beam splitters (SP2; Leica), which allowed excitation of X-rhod-1 (at 594 nm, with emission collected between 610 and 700 nm) alternating line by line with the excitation for D4cpv (at 458 nm, with emission collected between 470 and 510 nm for F_1 and 520 and 580 nm for F_2); therefore, images were effectively simultaneous. Interference between the two monitors (or their excitation

procedures) was explored in separate experiments in which one of the monitors was absent. No evidence of such interference was found. Various acquisition frequencies were used, depending on the duration of the pulses, so that resolution ranged from 1.25 to 5 ms per line (the alternate illumination resulting in actual intervals of 2.5–10 ms per line in the individual images). Spatial resolution was 0.24 µm/pixel. Line scanning was always parallel to the fiber axis at 10–15 µm from the glass coverslip.

The Forster resonant energy transfer (FRET) ratio R was calculated as $(F_2 - \text{Background}_2)/(F_1 - \text{Background}_1)$ without correction for non-FRET components in F_2. F_j could be a pixel value or an average. Background_i was measured with lasers off. $[Ca^{2+}]_{SR}$ was calculated from the ratio by a generalization of the equilibrium equation (Eq. 1 in Sztretye et al. [2011]) derived in the Appendix as

$$
(1)
$$
$$
[Ca^{2+}] = \beta K_d \frac{R - R_{\min}}{R_{\max} - R} + \frac{\beta}{k_{ON}}\left(\frac{dR}{dt}\right)\frac{R_{\max} - R_{\min}}{[R_{\max} - R + \beta(R - R_{\min})](R_{\max} - R)}.
$$

Here $\beta = F_1\, Ca^{2+}\text{-free}/F_1\, Ca^{2+}\text{-saturated}$. The parameter values of $R_{\min}$ (0.505), $R_{\max}$ (1.74), βK_d (222 µM), and β (0.554) were determined in calibrations in situ described in the companion paper (Sztretye et al., 2011). In 11 cells in which $[Ca^{2+}]_{SR}$ was followed dynamically, $R_{\min}$ was individually determined. This set of values was not significantly different from that found in the companion paper (Sztretye et al., 2011). Therefore, all calculations of $[Ca^{2+}]_{SR}$ were performed with the same set of parameter values. The stoichiometry factor n was set to 1 (as justified by Sztretye et al. [2011]). k_{ON} was assumed to be 3.6×10^6 $M^{-1}s^{-1}$, the value determined in solution at room temperature for the similar cameleon D1 (Palmer et al., 2004). Eq. 1 is identical to Eq. 6 in Wetzel and Gros (1998), which was applied in a study of Ca^{2+} transients monitored with fura-2.

Determination of free cytosolic $[Ca^{2+}]$: a calibration of X-rhod-1

Average cytosolic $[Ca^{2+}](t)$ is calculated from averaged fluorescence $F(t)$ as

$$
[Ca^{2+}]_c(t) = \frac{(F - F_{\min})k_{OFF} + dF/dt}{(F_{\max} - F)k_{ON}}. \tag{2}
$$

$F_{\max}$ and $F_{\min}$ are derived from Eq. 2 applied to the resting condition, in which $[Ca^{2+}]_c(0) \equiv [Ca^{2+}]_R$ is assumed equal to that in the pipette (0.1 µM; an assumption based on results by Royer et al. [2010]). Eq. 2 then becomes 0.1 µM $= (F - F_{\min})\, K_d/(F_{\max} - F)$.

In droplets of internal solution, $F_{\max}/F_{\min}$ was measured in our experimental setup as 157 for X-rhod-1 and 222 for Rhod-2. Affinity and kinetics were derived from dual line scans of fluorescence transients with X-rhod-1 and Rhod-2 in the same cell, releasing Ca^{2+} under a large and brief voltage clamp pulse. Line-averaged $F(t)/F_0$ in one such experiment is plotted in Fig. 1 A. Fluorescence of Rhod-2 was excited at 514 nm and collected in the range 540–570 nm; that of X-rhod-1 was as described in the previous subsection. Fig. 1 B plots with solid trace $[Ca^{2+}]_c(t)$ calculated from the fluorescence of Rhod-2 using Eq. 2, with $F_{\max}/F_{\min}$ determined in our experimental setup, $F_{\min}$ derived from F_0, the resting cytosolic $[Ca^{2+}]$ as

$$
F_{\min} = F_0 \frac{K_d + [Ca^{2+}]_c(0)}{K_d + [Ca^{2+}]_c(0) \times F_{\max}/F_{\min}}, \tag{3}
$$

and kinetic parameters provided by Escobar et al. (1997), including $K_d = 1.58$ µM and $k_{OFF} = 130$ s^{-1}. In the dashed trace is the corresponding calculation from the fluorescence of X-rhod-1, using
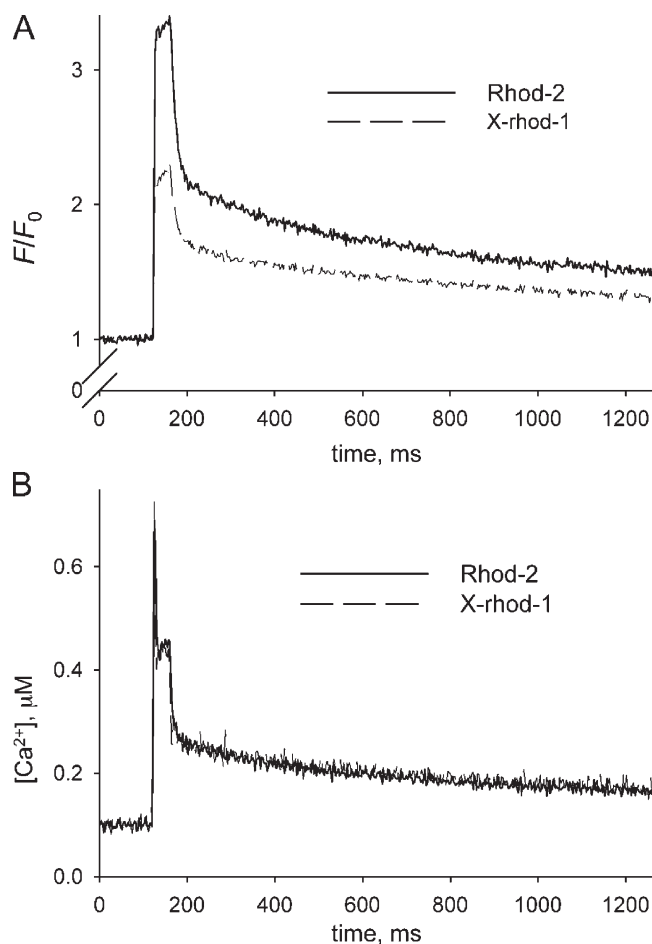
Figure 1. Kinetic parameters of X-rhod-1. (A) Baseline-normalized and line-averaged fluorescence F/F_0 of Rhod-2 and X-rhod-1 in a WT muscle cell subjected to a voltage clamp pulse of 50 ms to 30 mV. Fluorescence of Rhod-2 was excited at 514 nm and collected between 540 and 570 nm. The corresponding wavelengths for X-rhod-1 were 594, 610, and 700 nm. The excitation lights were interspersed line by line. (B, solid trace) $[Ca^{2+}]_c$ calculated from the fluorescence trace of Rhod-2 in A using Eq. 2, with F_{max}/F_{min} determined in our laboratory and kinetic parameters provided by Escobar et al. (1997), including K_d = 1.58 µM and k_{OFF} = 130 s^{-1}. (dashed trace) $[Ca^{2+}]_c$ calculated from the fluorescence trace of X-rhod-1 using Eqs. 2 and 3, with F_{max}/F_{min} determined in our laboratory and kinetic parameters adjusted for best fit to the function derived from Rhod-2. Best fit values were k_{ON} = 2.6 10^7 M^{-1}s^{-1} and k_{OFF} = 100 s^{-1}. ID: 031611b series 35.

measured F_{max}/F_{min}, F_{min} derived by Eq. 3, and kinetic parameters adjusted for best fit of the $[Ca^{2+}]_c$ waveform derived from Rhod-2 fluorescence. The best fit values were k_{ON} = 2.6 10^7 M^{-1}s^{-1} and k_{OFF} = 100 s^{-1} (for K_d = 3.9 µM).

In summary, X-rhod-1 proved to have both advantages and drawbacks compared with Rhod-2. Its spectra make it a good choice for joint use with fluorophores in the mid-wavelength range; it has a somewhat lower dynamic range (F_{max}/F_{min}), but its lower affinity results in a fairly linear relationship between signal and increase in $[Ca^{2+}]$ when millimolar concentrations of EGTA or BAPTA are present. Although its k_{ON} is substantially lower than that of Rhod-2, the good agreement between the waveforms of $[Ca^{2+}]_c$ derived from both dyes suggests that the interaction with cellular components does not introduce major qualitative changes

in its reaction with Ca^{2+} (or if it does, the changes are similar to those undergone by Rhod-2). This is different in the case of Fluo-4, the fluorescence transients of which could not be reconciled with those of Rhod-2 under the assumption of a binary Ca^{2+}:dye reaction of simple stoichiometry (Royer et al., 2008). Finally, it is worth noting that the derivation assumed a K_d of Rhod-2 determined in aqueous solution. If the affinity of Rhod-2 was lower inside cells, K_d of X-rhod-1 would be >3.9 µM.

The calculation of release flux

Ca^{2+} release flux $\dot{Rel}(t)$ was derived from $[Ca^{2+}]_c(t)$ by the removal method (Melzer et al., 1984, 1987), which calculates release flux as that necessary to account for the evolution of $[Ca^{2+}](t)$ in a single-compartment model that includes quantitatively specified processes of removal. Provided that $[EGTA]$ or $[BAPTA]$ are sufficiently high, only three removal processes must be considered: binding to the monitoring dye, binding to EGTA/BAPTA, and movement into the SR. This was performed here using the following parameter values: $[Dye]_{total}$, $[EGTA]_{total}$, and $[BAPTA]_{total}$ were set proportionally to the concentrations in the pipette and an exponential entry function of time described in the next subsection. As justified by Royer et al. (2008) and Schuhmeier and Melzer (2004), the kinetic constants of EGTA:Ca were k_{ON} = 15 (µM s)$^{-1}$ and k_{OFF} = 7.5 s^{-1}. For BAPTA:Ca, they were k_{ON} = 1,000 (µM s)$^{-1}$ and k_{OFF} = 200 s^{-1} (Wu et al., 1996). k_{uptake}, the proportionality constant linking the rate of pump removal to $[Ca^{2+}]_c$, was allowed to vary among cells for best fit of $[Ca^{2+}]_c(t)$. The best fit value varied in the range 3.5–26 ms^{-1}, with an average of 10.1 ms^{-1} (SEM = 1.37 ms^{-1} in 51 cells).

The images were obtained at 2.5 –10 ms/line. The peak value of release flux was corrected for the blunting effect of these low sampling rates using empirical factors derived as described by Royer et al. (2008), who also showed that measures of the amplitude of release flux at more slowly varying milestones during a long-lasting depolarization do not change with acquisition rate. Given the large blunting effect of the low frequencies used for scanning, the values of peak flux, even after correction, should be viewed as rough approximations.

Entry of buffers into cells

The quantitative analysis of flux requires knowledge of the concentration of the main buffer at any point in time. Strictly, the cytosolic concentrations of BAPTA or EGTA remain unknown. For an objective estimate, we assumed an entry function that depends exponentially on time since whole-cell patching. Namely,

$$[Buffer](t) = a + ([Buffer]_{pipette} - a)(1 - e^{t/\tau}),$$

where a is a small negative constant of convenience and τ equals 37.5 min for BAPTA and 34.8 min for EGTA. These values were adapted from an average estimate of EGTA entry by Schuhmeier et al. (2005). The slight difference between time constants of BAPTA and EGTA was calculated assuming inverse proportionality between τ and diffusion coefficient D and inverse proportionality between D and molecular radius, which was calculated from the molecular weight.

It should be stressed that any binding of the buffer to cellular structures will increase the asymptotic value of $[Buffer]$ above $[Buffer]_{pipette}$ and will also change its effective diffusion coefficient. Binding might additionally change reaction kinetics and K_d. Therefore, the values of flux and amount of Ca^{2+} released will remain subject to an error of scale, roughly proportional to the error in $[Buffer]$. If the diffusion of the buffer or its kinetics is substantially different than assumed here, the error will be time dependent. The present work focuses on the differences introduced by genetic modification; thus, the possible errors of scale or kinetics should not severely qualify the main conclusions and outcomes.

Amount released

From $\dot{Rel}(t)$, which is the flux calculated to exit exclusively through release channels, a magnitude $\dot{R}_{net}(t)$ quantifying the net flux leaving the SR is derived by subtraction of the pump removal flux, namely

$$\dot{R}_{net}(t) = \dot{Rel}(t) - k_{\text{uptake}}[Ca^{2+}]_c(t).$$

The difference between $\dot{Rel}$ and $\dot{R}_{net}$, which is proportional to $[Ca^{2+}]_c$, is almost negligible in the highly buffered conditions of this study. The integral, from the beginning of the pulse until time t, defines $Rel(t)$, the amount released at time t.

$$Rel(t) \equiv \int_0^t \dot{R}_{net}(u)du. \qquad (4)$$

This integral, extended to the time when net flux vanishes by depletion, defines $Rel(\infty)$, the SR content releasable by depolarization.

Transgenic animals

Mice lacking Casq1 (Paolini et al., 2007) were raised at Charles River and used at 6–10 wk of age.

Online supplemental material

The supplemental text includes an example cell in which SR depletion results in a signal of dynamic range ($\Delta R/R_{\min}$) much greater than in published observations and also contains an analysis of causes of error in a previous estimate of the change in evacuability during a depleting depolarization. Fig. S1 shows the signal with high dynamic range. Fig. S2 examines the error in the estimation of evacuability. Online supplemental material is available at http://www.jgp.org/cgi/content/full/jgp.201010592/DC1.

RESULTS

In this section, we present direct measurements of the changes in cytosolic $[Ca^{2+}]$ elicited by voltage clamp depolarization of skeletal muscle cells, together with simultaneous measurements of $[Ca^{2+}]$ in the SR lumen. The cytosolic transients are used to derive Ca^{2+} release flux and its evolution during depolarizations that last a time sufficient to reach a steady $[Ca^{2+}]_c$ (and presumably a steady level of depletion of Ca^{2+} in the SR).
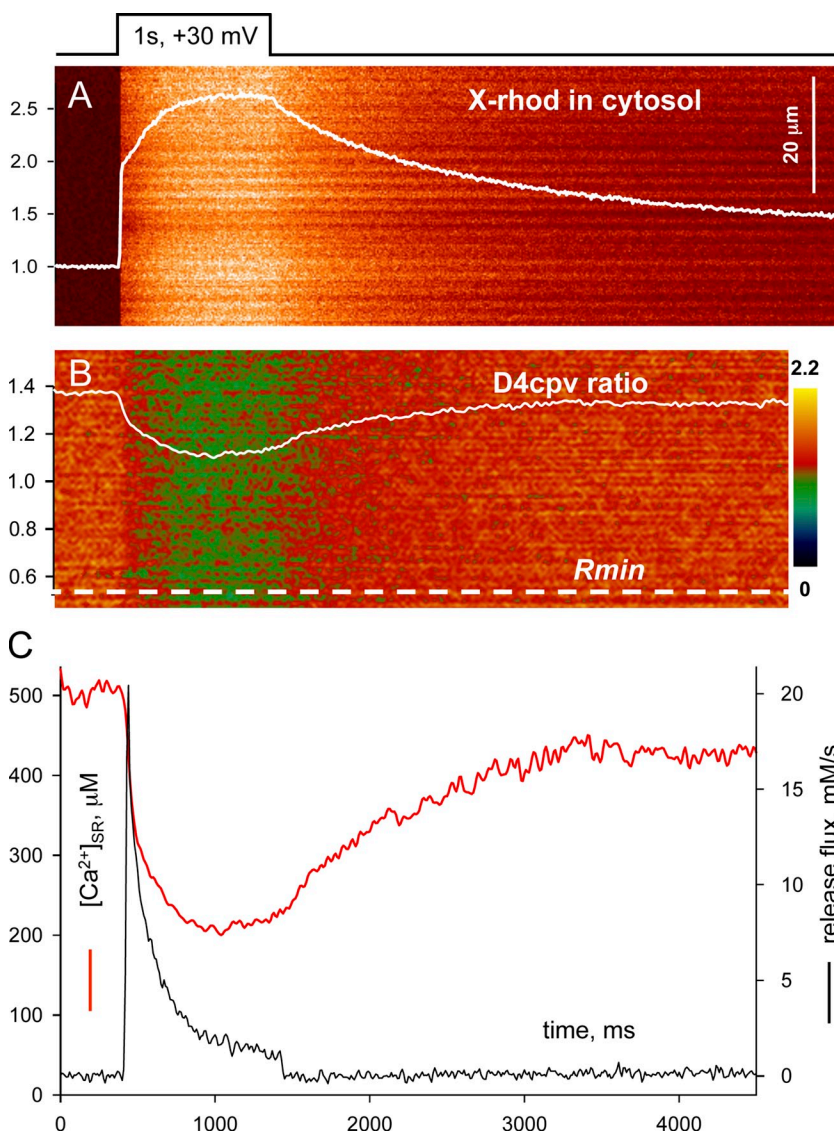
Figure 2. Simultaneous determination of $[Ca^{2+}]_c(t)$ and $[Ca^{2+}]_{SR}(t)$ in a muscle cell. (A) Fluorescence of X-rhod-1 in cytosol. Cell perfused with EGTA solution subjected to the voltage clamp pulse drawn at top. Fluorescence was normalized to resting time average $F_0(x)$. The plot is of spatially averaged $F(t)/F_0$. (B) $R = F_2(x,t)/F_1(x,t)$ of simultaneously recorded line scans of fluorescence of the biosensor, D4cpv-Casq1 in this case, with specific wavelengths of excitation and emission given in Materials and methods. The plot is of spatially averaged R. The dashed line marks $R_{\min}$. (C) Plots of release flux (black) calculated from $F(t)/F_0$ and $[Ca^{2+}]_{SR}$ (red) calculated from $R(t)$ by Eq. 1. The final $[Ca^{2+}]_{SR}$ level reached during this depolarization is close to the average (namely 179 µM; listed in Table I). ID: 072309a_series106. Average of six line scans obtained with 3-min intervals at between 130 and 145 min after establishing whole-cell patch is shown.

The results are compared under four circumstances, arising from the combination of two binary changes: one is the alternative use of two extrinsic and dominant buffers (EGTA or BAPTA), and the other is the use of cells from wild-type (WT) mice or cells from the Casq1-null murine strain.

Change in $[Ca^{2+}]_{SR}$ upon depolarization-induced Ca^{2+} release

The evolution of $[Ca^{2+}]_{SR}$ during Ca^{2+} release induced by long-lasting depolarizations (0.4–1.5 s) to a maximally activating voltage was followed in cells of muscles expressing the biosensor D4cpv-Casq1 or D4cpv-δAsp. The cytosol was loaded with the Ca^{2+}-sensitive dye X-rhod-1, which diffused from the patch pipette. The image of X-rhod fluorescence was acquired in parallel with the FRET image pair (F_1 and F_2) required to calculate $[Ca^{2+}]_{SR}$. Fig. 2 A, illustrating images from a cell expressing D4cpv-Casq1, shows normalized fluorescence of the cytosolic dye ($F(x,t)/F_0(x)$) and a superimposed plot of the spatial average $F(t)/F_0$. In Fig. 2 B, $R \equiv F_2(x,t)/F_1(x,t)$ is shown (see Materials and methods). This ratio depends monotonically on $[Ca^{2+}]_{SR}$, which is derived from R by Eq. 1. It can immediately be seen that in this cell the ratio decreased, concomitantly with Ca^{2+} release, but the value reached after prolonged depolarization was far from the minimum. Fig. 2 C summarizes the analysis of the line scans. In black is the Ca^{2+} release flux, $\dot{Rel}(t)$, derived from the fluorescence of the cytosolic dye. It shows the usual features: initial peak, which at this sampling rate is poorly resolved, followed by a slower phase of decay that includes a "shoulder" (described by Royer et al. [2008, 2010] and more prominently seen in a later example). In red is $[Ca^{2+}]_{SR}$, which tends to stabilize after prolonged depolarization at a value that is ∼35% of the resting $[Ca^{2+}]_{SR}$. Table I lists averages of initial and final values of $[Ca^{2+}]_{SR}$, as well as key parameters of flux.

Depletion is much greater in Casq-null cells

In WT muscle fibers, depletion reached by maximally activating depolarization is partial, to 35% of initial concentration. As shown later, this requires actual turn-off of the release channels, which is likely induced by the lowered $[Ca^{2+}]_{SR}$. An analogous shut off by lumenal $[Ca^{2+}]$ is thought to take place and be mediated by Casq in cardiac muscle (Györke et al., 2009). We tested the presence of this mechanism in skeletal muscle by repeating the measurements in muscle fibers of mice null for Casq1. In a representative cell, it can bee seen that the flux ($\dot{Rel}(t)$; Fig. 3 C, black trace) in Casq-1 nulls differs from the corresponding transients in WT as previously described by Royer et al. (2010). Most visible is the hastening of the decay, which goes from a time constant of 323 ms in the WT example of Fig. 2 to 77 ms in Fig. 3.

In addition, major changes are found in the extent and rate of the decrease in $[Ca^{2+}]_{SR}$. To facilitate the comparison, Figs. 2 B and 3 B are presented with the same color scale. Clearly, the depletion reached in the null cell was much greater, with the final level reaching <30 µM. An even greater descent, which is also notable for having started from a higher resting $[Ca^{2+}]_{SR}$, is illustrated in Fig. S1. On average in eight cells, the final value was 39 µM (Table I). This average is approximately five times lower than the corresponding value in the WT, and the difference is highly significant.

The kinetics of release flux is altered by a fast buffer

The observations on the Casq-null cells were consistent with the hypothesis that the channels close to terminate release and that this closure somehow requires the presence of Casq. One aspect of this model, as currently understood in cardiac muscle (Györke et al., 2009; Zima et al., 2010), is that the primary variable is $[Ca^{2+}]_{SR}$, which determines closure of channels upon reaching a threshold low value. This hypothesis requires that release transients terminate at a set level of

TABLE I
Evolution of FRET ratio and properties of Ca^{2+} release flux

Conditions	R initial	R final	Peak flux	Amount	$[Ca]_{SR}$ initial	$[Ca]_{SR}$ final	n cells
			$mM\ s^{-1}$	μM	μM	μM	
WT EGTA	1.32 (0.03)	1.04 (0.03)	54.6 (9.7)	1,926 (259)	507 (99.0)	179 (19.3)	14
WT BAPTA	1.26 (0.04)	1.07 (0.05)	119 (11.8)[a]	1,093 (65.9)[a]	437 (54.1)	201 (26.8)	22
All WT	1.28 (0.03)	1.06 (0.03)	94.0 (9.6)	1,416 (126)	464 (50.2)	207 (18.6)	36
Null EGTA	1.25 (0.07)	0.68 (0.04)[b]	43.4 (6.7)	1,189 (174)[b]	448 (111)	39 (9.99)[a]	9
Null BAPTA	1.35 (0.04)	0.74 (0.04)	115 (15.3)[a]	982 (78.8)	604 (100)	59 (8.30)[a]	14
All null cells	1.32 (0.04)	0.72 (0.03)[b]	89.2 (12.4)	1,061 (82.7)[b]	547 (75.2)	51 (8.46)[a]	23

Effects of long lasting depolarization are shown. The second column shows initial FRET ratio in resting cells. The third column shows steady value of ratio reached after a pulse to 30 mV, 0.4–0.5 s long in experiments with BAPTA or 1–1.5 s in experiments with EGTA. Note that R initial is approximately the same for different preparations, but the extent of decay (depletion) is much greater in Casq-null cells. The fourth and fifth columns show peak Ca^{2+} release flux and amount released after the maximal long-lasting pulse. Note significantly greater peak flux in BAPTA but no difference in peak flux values between WT and nulls. Amount released is decreased in the null cells by about 30%. The sixth and seventh columns show initial and final values of $[Ca^{2+}]_{SR}$, calculated from corresponding R values. SEM values are shown in parentheses.
[a]Values in BAPTA are significantly different from those in EGTA.
[b]Values in null are significantly different from those in WT.

$[Ca^{2+}]_{SR}$, regardless of the release history or kinetics whereby such level was reached (a prediction that was recently tested in cardiac muscle by Zima et al. [2010], with positive results). The hypothesis was tested in this study through the introduction of a different exogenous Ca^{2+} buffer.

BAPTA has an affinity for Ca^{2+} similar to that of EGTA and two orders of magnitude faster kinetics of reaction (e.g., Wu et al., 1996). Its substitution for EGTA is a well established test for the presence of Ca^{2+}-dependent inactivation (CDI), which may be reduced in the presence of BAPTA at high concentrations. In these tests, we used 5 mM BAPTA, which under current estimates of K_d results in an equilibrium buffer power similar to that of 10 mM EGTA present in our reference medium.

Fig. 4 shows Ca^{2+} transients recorded in the same manner as in the previous experiments in WT muscle fibers, after ~1 h of equilibration with BAPTA in the patching pipette. Under this condition, $\dot{Rel}(t)$ became greater and faster changing. Although in EGTA it takes ~200 ms for flux to decay to half-value in its quasi-steady phase (Royer et al., 2010), this decay took <50 ms in BAPTA. For this reason, the duration of the pulses was reduced to 400 ms, which left more time for recovery and signal averaging, and the display time scales were adjusted accordingly. As can be seen in the flux record (Fig. 4 C, black trace) and confirmed in Table I, with BAPTA in the pipette, $\dot{Rel}(t)$ peaked at a more than two-fold greater value than in the presence of EGTA and displayed a prominent shoulder at 25–40 mM/s, a shoulder which was often pinched in the shape of a hump or secondary increase. The most prominent difference in BAPTA, though, was the very rapid decay of $\dot{Rel}(t)$ to a low steady level, decay which in most cases took <100 ms.
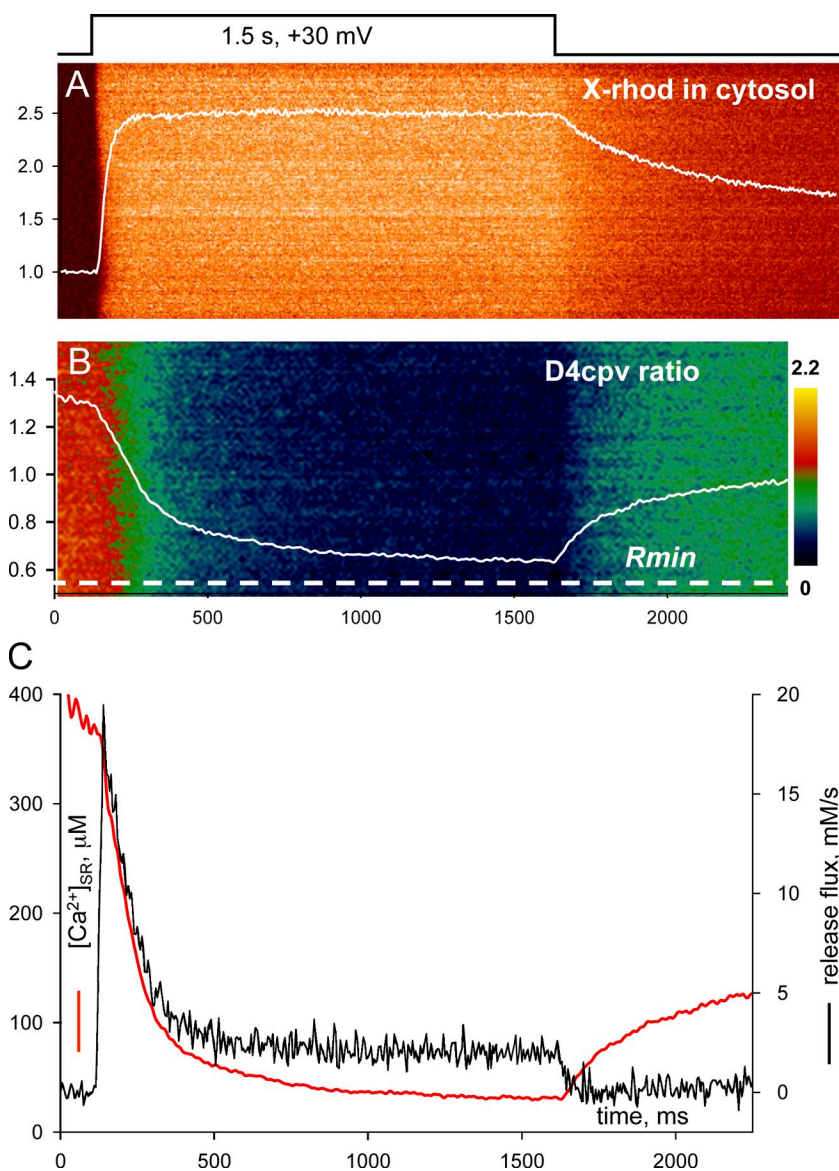

Figure 3. Simultaneous determination of $[Ca^{2+}]_c(t)$ and $[Ca^{2+}]_{SR}(t)$ in a Casq1-null cell. (A) Fluorescence of cytosolic monitor in cell perfused with EGTA. (B) $R(x,t)$ and (in white trace) its line average $R(t)$. The dashed line marks R_{min}. (C) Release flux (black) and $[Ca^{2+}]_{SR}(t)$ (red). Details of description were given in legend of Fig. 2. Note the greatly increased degree of depletion by the end of the pulse. Also note the continued decrease of $R(t)$ during the pulse, contrasting with stabilization in the WT (Fig. 2). ID: 062410a _s34. Average of eight line scans obtained 31–51 min after establishing whole-cell patch is shown.

In correspondence with the faster flux, $[Ca^{2+}]_{SR}$ decayed more abruptly in BAPTA but did not reach substantially lower levels than when EGTA was used as buffer (Table I). In the Casq-null cells, illustrated in Fig. 5, BAPTA had a similar effect: it enhanced $\dot{Rel}(t)$ and accelerated depletion of the SR, but the final $[Ca^{2+}]_{SR}$ reached was similar to that in the null cells in EGTA, as was the case for WT cells.

Voltage-dependent inactivation of the voltage sensor

The results of the previous section show that release flux decreases substantially after partial SR depletion, with half-times of 50–200 ms (depending on the buffer present intracellularly). One of the possible causes of reduction of Ca^{2+} release is inactivation of the t tubule voltage sensor, the dihydropyridine receptor, which in addition to disabling the release response manifests itself by substantial reduction of the amount of intramembranous charge mobile in the voltage range in which the functional response is elicited. In mouse fast-twitch muscle, intramembranous charge displacement Q_m and release flux were first measured in detail by Ursu et al. (2005), who found that $Q_m(V_m)$ was described

approximately by a Boltzmann function with transition voltage $V_T = -14$ mV, and flux depended on voltage in a similar way, but its transition voltage was ~6 mV more positive.

In voltage clamped flexor digitorum brevis (FDB) cells, we recorded charge movement current I_Q and computed Q_m to evaluate the effects of a prior depolarization. The results are illustrated in Fig. 6. At the top is I_Q in test depolarizations to a variable level V_m, applied from rest or after a conditioning depolarization of 400 ms, which is a duration chosen to be in excess of the times of interest. Fig. 6 B plots Q_m versus V_m in the range 0–40 mV for the same cell, with Q_{ON} represented by closed symbols, Q_{OFF} by open symbols, and the conditioned values in red. Q_{OFF} values, which are similar to Q_{ON} for pulses up to 0 mV, become progressively greater at $V_m > 0$ mV, which is an indication that large test voltages activate ionic currents that interfere with the measurement of Q_m.

The conditioning depolarization (currents and symbols in red) caused changes in the distribution, including a decrease by 20% of Q_{max}, the maximum of the Boltzmann fit to Q_{ON}. However, Q_m values were actually affected only at voltages >0 mV. This suggests that the
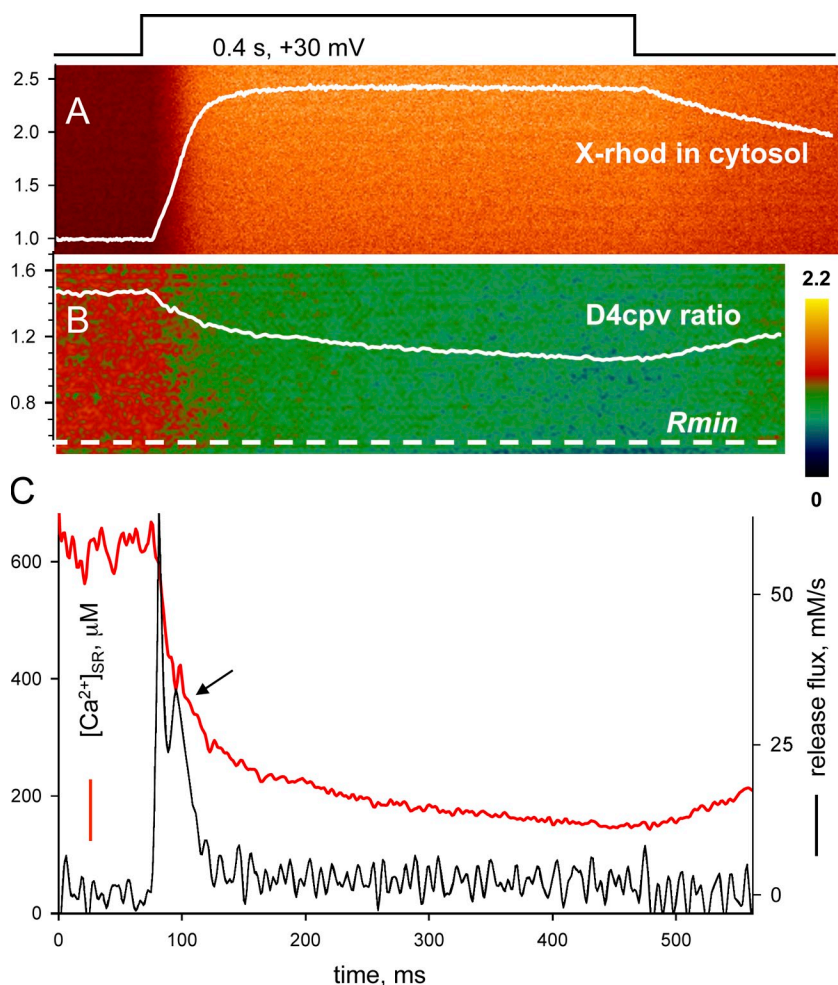

Figure 4. $[Ca^{2+}]_c(t)$ and $[Ca^{2+}]_{SR}(t)$ in a WT cell with BAPTA. (A) Fluorescence of X-rhod-1. (B) $R(x,t)$ and (in white trace) its line average $R(t)$. (C) Plots of release flux and $[Ca^{2+}]_{SR}(t)$ as in Figs. 2 and 3. Internal solution was BAPTA. Note the radical changes in amplitude and kinetics of flux compared with Fig. 2, most notably an increase in peak and intermediate level, with a reduction in duration of the intermediate stage and the appearance of a hump (arrow). Also note a greatly expanded temporal scale, to better display the hastened kinetics. ID: 051209b _s43. Average of 13 line scan images taken 47–72 min after patching is shown.
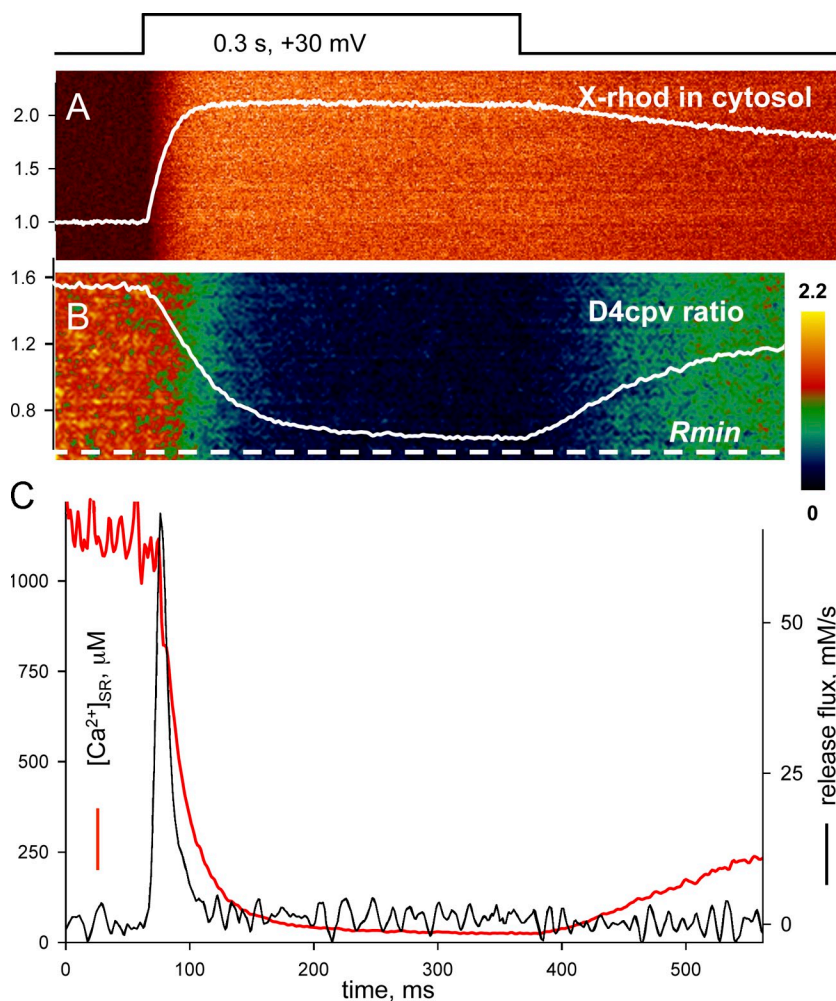
Sztretye et al. 237

Figure 5. [Ca^{2+}] in cytosol and SR in a Casq-null cell with BAPTA. (A) Fluorescence of X-rhod. (B) $R(x,t)$ and (in white trace) its line average $R(t)$. (C) Release flux (black) and [Ca^{2+}]$_{SR}(t)$ (red). Details of description were given in legend of Fig. 2. Note the rapid stabilization of fluorescence in the cytosol and rapid decay of release flux to very low levels, which is a consequence of the presence of BAPTA. Also note the lack of any shoulder or hump in the evolution of release flux and the drastic decay of [Ca^{2+}]$_{SR}$ to nearly 0, which is a consequence of the absence of Casq. ID: 082009b_s34. Average of 10 line scan images taken 48–68 min after patching is shown.

effects observed at positive V_m reflect an alteration of ionic currents more than a true inactivation of voltage sensors.

Q_m averaged over 10 experiments at test voltages of 0 mV or lower is plotted in Fig. 6 C. In this range of V_m, the averages of Q_{ON} and Q_{OFF} are not significantly different; this suggests that the displacements are well determined,

with little interference by asymmetric ionic currents. The charge displaced by test pulses preceded by the conditioning depolarization (red symbols) was statistically not different from the reference values at any potential within this range. Considering that the transition voltages of both charge movement and release activation are <0 mV (e.g., Ursu et al., 2005), the results imply

TABLE II

Testing whether EC coupling properties are altered by exogenous Casq

Conditions	R initial	R final	Peak flux	Amount	[Ca]$_{SR}$ initial	[Ca]$_{SR}$ final	n cells
			$mM\,s^{-1}$	μM	μM	μM	
WT EGTA Casq	1.33 (0.05)	1.06 (0.04)	61.2 (12.8)	2,197 (320)	547 (138)	183 (25.8)	10
WT EGTA δAsp	1.29 (0.02)	1.04 (0.06)	38.0 (8.44)	1,246 (185)	407 (23.0)	170 (24.7)	4
WT BAPTA Casq	1.29 (0.04)	1.05 (0.05)	123 (12.8)	1,191 (76.5)	448 (58.9)	201 (26.8)	14
WT BAPTA δAsp	1.22 (0.08)	1.12 (0.07)	113 (24.5)	920 (101)	416 (113)	263 (59.7)	8
Null EGTA Casq	1.16 (0.18)	0.63 (0.08)	46.3 (15.2)	947 (88.6)	404 (259)	27.7 (18.7)	3
Null EGTA δAsp	1.31 (0.06)	0.71 (0.05)	41.7 (7.39)	1,334 (265)	475 (117)	45.3 (12.1)	6
Null BAPTA Casq	1.38 (0.06)	0.70 (0.08)	86.3 (19.8)	1,139 (70.6)	658 (144)	51.6 (24.6)	6
Null BAPTA δAsp	1.33 (0.05)	0.78 (0.03)	137 (19.9)	848 (114)	564 (144)	65.7 (9.27)	8

Definitions of values in columns are as in Table I. Groupings of cells in Table I are further separated depending on the Casq variant fused to the biosensor. No significant differences were found in the properties of [Ca^{2+}]$_{SR}$ and release flux between cells expressing D4cpv-Casq1 and D4cpv-δAsp. SEM values are shown in parentheses.
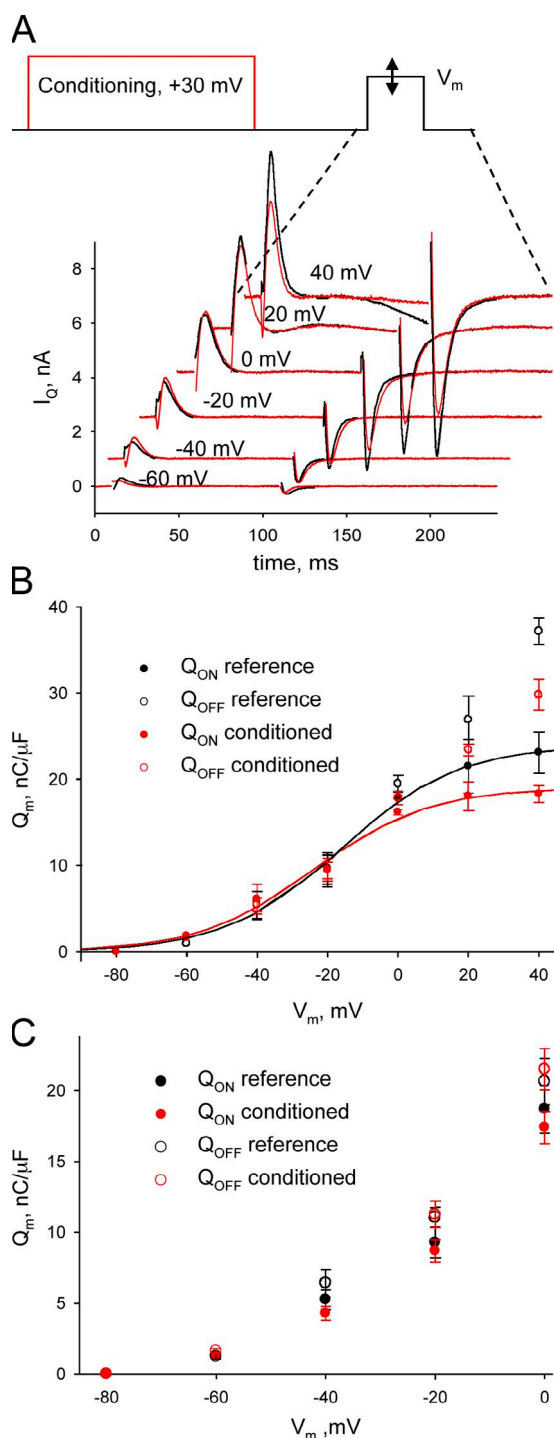
Figure 6. Effects of a conditioning depolarization on the t tubule voltage sensor. (A) Intramembranous charge movement currents I_Q in test depolarizations to a variable level V_m applied from rest or after a conditioning depolarization (diagram at top). (B) Charge displacement Q_m versus V_m in the range 0–40 mV for the same cell, with displacement during the ON (Q_{ON}) represented by closed symbols, Q_{OFF} values by open symbols, and the conditioned values in red. Q_{OFF} values become progressively greater than Q_{ON} at $V_m > 0$ mV, which is an indication that large test voltages activate ionic currents that interfere with the measurement of Q_m. The continuous curves plot Boltzmann fits $Q_{ON} = Q_{max}/(1 + \exp(-(V_m - V_T)/K))$. In reference (black), the parameter values were $Q_{max} = 24.0$ nC/μF,

that charge movement of the voltage sensor is minimally affected. In conclusion, voltage-dependent inactivation cannot be a major determinant of the drastic decay in flux demonstrated in the previous sections. These results are therefore compatible with every component of the working hypothesis: channels close during long-lasting Ca^{2+} release, the change is brought about by reduction of $[Ca^{2+}]_{SR}$ below a certain threshold, and this effect requires the presence of Casq, presumably as an allosteric transducer of the change in $[Ca^{2+}]_{SR}$.

Effects of the presence of the biosensor

A major advantage of the present approach to measuring $[Ca^{2+}]_{SR}$ is the almost perfectly selective targeting of the biosensor to the SR, provided by the fused Casq1. This approach has, of course, the disadvantage of adding exogenous, fused Casq1 to the native SR endowment. We tested for effects of the extrinsic Casq in two ways: using D4cpv fused to a variant of Casq1 with impaired Ca^{2+} binding (Shin et al., 2000) and using the naturally occurring intracell heterogeneity in density of biosensor expression, which results in changes in local biosensor concentration by up to 10-fold.

All aforementioned experimental combinations between WT and null cells, as well as between cells perfused with EGTA and cells with BAPTA, were performed as two sets of experiments, one using D4cpv-Casq1, with the native Casq sequence, and another using D4cpv-δAsp. The averaged results for all sets are listed in Table II. The database presented in both Tables I and II is the same, the single difference being the separation by biosensor variant in Table II. Therefore, all differences already described between WT and null and between flux characteristics in the two buffers are also contained in Table II and are not marked. Data in Table II reveal virtually no differences in either flux or depletion characteristics attributable to the use of different variants of the biosensor. Thus, this analysis validates the approach used in Table I of grouping results obtained with both variants of the biosensor. Other implications of this negative result will be described in the Discussion.

The second evaluation of potential buffering effects of the extrinsic Casq is illustrated in Fig. 7. In Fig. 7 A is the invariant image of biosensor in a cell, obtained by combination of F_1 and F_2 according to Eq. A6 of Sztretye et al. (2011). The intensity of this image is proportional

$V_T = -16.4$ mV, and $K = 16.5$ mV. After conditioning (red) $Q_{max} = 19.0$ nC/μF, $V_T = -20.3$ mV, and $K = 16.3$ mV. ID: 1066E. (C) Q_m averaged over 10 experiments at test voltages up to 0 mV. Symbols and colors are as described for B. Error bars represent SEM. In this range, the averages of Q_{ON} and Q_{OFF} were not significantly different, and the changes induced by the conditioning depolarization were not significantly different from zero. ID: 1059E through 1069E (excludes 1062E).

to biosensor concentration, scaled according to the color table in micromoles of protein per liter of cell. In Fig. 7 B is the ratio image, $R(x,y)$, at rest. The histogram of this image, in Fig. 7 C, is narrow, which is consistent with a FRET ratio that is nearly constant and therefore essentially independent of biosensor concentration. (An exception is the perinuclear area, where biosensor concentration is extremely high and R is slightly lower, a trend evaluated by our companion paper [Sztretye et al., 2011], in which we showed that the slight variation was probably related to local changes in the properties of the biosensor, rather than in $[Ca^{2+}]_{SR}$).

The functional properties of regions with different concentrations of the fusion protein were compared in simultaneous line scans of fluorescence of biosensor and cytosolic dye, which in the example were obtained at or near the dashed line in Fig. 7 A. Two regions of the line scans, marked as "a" and "b" by segments below Fig. 7 A, were averaged and processed separately, with results plotted in the figure. The average concentrations of biosensor were 1.54 µM and 7.54 µM, respectively, in a and b. The observations with the cytosolic monitor are illustrated in Fig. 7 (E and F); $\dot{Rel}(t)$ was essentially identical in the two regions. The evolution of amount released,
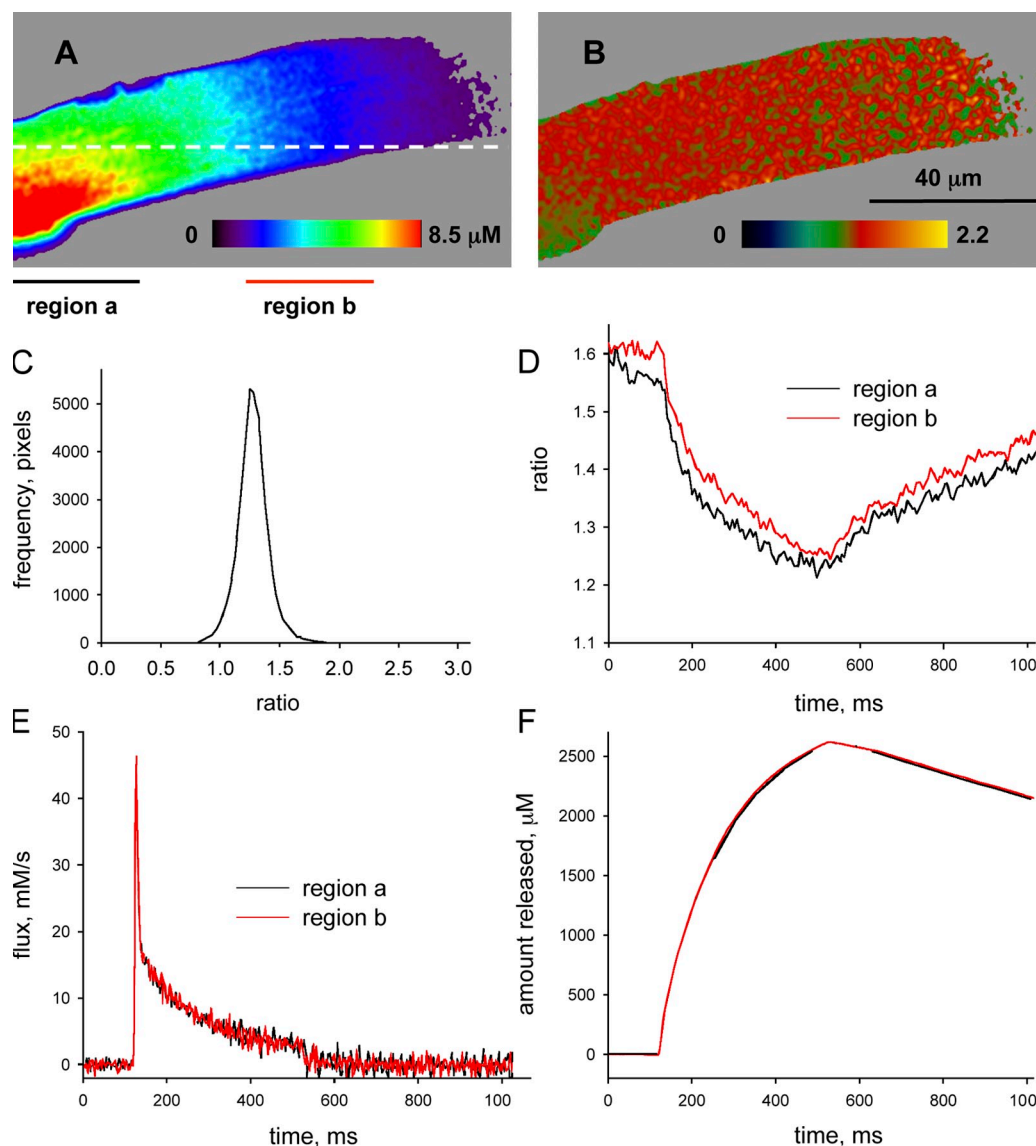

Figure 7. Release flux and FRET ratio in a cell with spatially heterogeneous biosensor expression. (A) Biosensor concentration (invariant image) calculated as described in Eq. A6 of Sztretye et al. (2011). (B) FRET ratio R. (C) Histogram of pixel values of R. The distribution is narrow, which is consistent with a lack of effect on R of the variation in [biosensor]. (D) $R(t)$ in line scans along dashed line in A, averaged over regions a (high [biosensor]) and b (low) indicated by line segments at the bottom of A. The average concentration of biosensor was 7.54 µM and 1.54 µM, respectively, in a and b. Note slightly greater R in region b. (E and F) $\dot{R}_{net}(t)$ and its integral $Rel(t)$ (Eq. 4) in regions a and b. No difference is visible in spite of the large change in biosensor concentration. ID: 072309a image 29.

Rel(*t*), in Fig. 7 F, was also nearly identical in regions a and b. This similarity is especially meaningful because *Rel*(*t*), which is the integral of net flux (Eq. 4), should reveal any significant difference better than the noisy *Ṙel*(*t*) records. Evidently none existed in this case.

As described in the companion paper (Sztretye et al., 2011) and exemplified in the present case by the graph in Fig. 7 D, a small difference in *R*, of ∼0.03 in the example, was frequently observed in favor of the regions of lower biosensor concentration. As shown, the difference was essentially constant during concentration transients, suggesting a shift in optical properties of the biosensor.

Based on different observations, it therefore appears that the fusion of Casq1 and biosensor, expressed within the present concentration range in WT cells, does not interfere with the Ca^{2+} movements of excitation–contraction coupling (EC coupling). This conclusion does not exclude the possibility of buffering effects of the biosensor when it is expressed in Casq-null cells.

DISCUSSION

In this study, the flux of voltage-induced release of Ca^{2+} into the cytosol and the free SR $[Ca^{2+}]$ were simultaneously monitored in skeletal muscle cells. Because this is to our knowledge the first study to date that combines both measurements in skeletal muscle, its focus has been narrowly defined, leaving for future work many other questions that can be addressed with the present techniques.

The first observation made was that the depletion of SR Ca^{2+} caused by membrane depolarization is limited in WT cells. Specifically, the release of Ca^{2+} induced by continuous membrane depolarization at levels that maximally activate the release process resulted in the free $[Ca^{2+}]$ of the SR stabilizing at ∼35% of the initial value, measured in the cells at rest. Roughly, $[Ca^{2+}]_{SR}$ started at 500 μM, or a bit less, and stabilized at between 150 and 200 μM, after continued release for ∼0.5 s. The observation implies that release channels close before depletion is complete. Measurement of intramembranous charge movement, which is largely a manifestation of the voltage-sensing function of the dihydropyridine receptor, failed to show a significant reduction of charge displacement by the depolarizations, which rules out inactivation of the voltage sensor as a major determinant of the channel closure.

The observation is consistent with prevailing ideas of control of Ca^{2+} release in cardiac muscle (as recently elaborated by Zima et al. [2010]), whereby ryanodine receptor (RyR) channels close and terminate Ca^{2+} release when $[Ca^{2+}]_{SR}$ reaches a threshold value in a control process mediated by Casq and perhaps requiring other junctional proteins.

Two aspects of this mechanism were tested in this study. Depletion measured under the same protocol was found to be much more complete in Casq1-null mice than in the WT. The final level of $[Ca^{2+}]_{SR}$ reached after prolonged depolarization in the null muscles was measured at between 10 and 60 μM.

An additional prediction was tested, that release must terminate at a fixed level of $[Ca^{2+}]_{SR}$, regardless of the path or history of Ca^{2+} release that caused $[Ca^{2+}]_{SR}$ to reach that level. The prediction was tested by substitution of BAPTA for EGTA in the internal solution, a maneuver predicted to change release flux by interfering with CDI of the release channels. This had the expected effect, making *Ṙel*(*t*) substantially greater, both at its peak and its intermediate or shoulder stage.

As a consequence of the increase in *Ṙel*(*t*), the $[Ca^{2+}]_{SR}$ level associated with release termination in EGTA was reached much sooner in BAPTA. Termination of release occurred at this much earlier time, in agreement with the hypothesis that the trigger for termination is the attainment of a certain value of SR lumenal $[Ca^{2+}]$. All observations are therefore consistent with the notion that $[Ca^{2+}]_{SR}$ reduction below ∼150 μM results in a signal for channel closure, a signal which requires the presence inside the SR of Casq, presumably acting as an allosteric sensor of the fall in $[Ca^{2+}]_{SR}$.

Permeability to Ca^{2+} of the SR membrane decreases upon depletion

A quantitative representation of the changes induced by depletion is provided by the evaluation of permeability to Ca^{2+} of the SR membrane, an evaluation which the new tool allows us to do directly, without resorting to model-dependent guesses about the evolution of the Ca^{2+} gradient. The algebra of the measurement is simple. Membrane permeability is defined as

$$P \equiv \frac{\text{amount}/(t.A_{SR})}{[Ca^{2+}]_{SR} - [Ca^{2+}]_c}, \quad (5)$$

where A_{SR} represents SR membrane area, the numerator is flux per unit area, and the denominator is the $[Ca^{2+}]$ gradient. Then the ratio of measured flux to measured gradient is proportional to P, namely

$$\frac{\dot{Rel}}{[Ca^{2+}]_{SR} - [Ca^{2+}]_c} \approx \frac{\dot{Rel}}{[Ca^{2+}]_{SR}} =$$

$$= \frac{A_{SR}.\text{amount}}{A_{SR}.t.\,V_c.[Ca^{2+}]_{SR}} = \frac{A_{SR}}{0.7V}P.$$

Here the free cytosolic Ca concentration $[Ca^{2+}]_c$ has been neglected by comparison with $[Ca^{2+}]_{SR}$, and the cytosolic volume V_c has been equated to 0.7 of the cell volume V (0.865 is the fraction of mouse fiber volume

outside mitochondria and SR [Eisenberg, 1983]; Baylor et al. [1982] calculate the water content of frog muscle fibers as 0.810 gm/cm³; an approximate number for the fractional volume of water outside the SR and mitochondria is therefore 0.865×0.810 gm/cm³ $= 0.701$). The measurable variable is $\dot{Rel}/[Ca^{2+}]_{SR}$, with dimensions of inverse time (units are s⁻¹). Following common usage, this measurable variable will be loosely referred to as "permeability," with the underlying assumption that the factor relating it to actual permeability $(A_{SR}/(0.7V))$ remains constant.

Permeability, thus calculated for the four experimental example cases, is plotted in Fig. 8. The records for WT are in black trace, and those of null muscle cells are in red. In both EGTA (Fig. 8 A) and BAPTA solutions (Fig. 8 B), permeability in WT cells decays markedly during the pulse but does so much more rapidly in BAPTA (Table I). The corresponding records in Casq-null cells evolve either without the marked decrease (Fig. 8 A) or show a decay in permeability that is transient (Fig. 8 B). In every Casq1-null cell examined, the final level of permeability was several times greater than that in the WT cells at comparable times.

The striking difference in the evolution of permeability between WT and nulls could have been predicted from the different final degree of depletion. Indeed, it has already been shown that the final (steady or cycling) levels of flux are similar in WT and Casq-null cells (Royer et al., 2010). Therefore, the approximately equal flux requires greater permeability in the nulls given their greater degree of depletion.

It is noteworthy that the difference in P between WT and null is reflected in the final level of $[Ca^{2+}]_{SR}$ but not in the final flux level. This result suggests that the main contributors to the steady movements of Ca^{2+} after a long-lasting depolarization are SR to cytosol flux through RyRs and removal by SERCA. In turn, this removal flux is largely determined by the steady cytosolic $[Ca^{2+}]$ level, which does not differ substantially between WT and null cells. The release flux through RyRs, which must be equal and opposite in the steady situation, settles at the same value as in the WT, a value resulting from a smaller gradient and a greater permeability.

Measurements with cameleon biosensors are in qualitative agreement

The present results can be compared with earlier studies. Working on toad muscle, Kabbara and Allen (2001) used SR-loaded fluo-5N to dynamically monitor for the first time the evolution of $[Ca^{2+}]_{SR}$ during the EC coupling process. They reported a 33% reduction in $[Ca^{2+}]_{SR}$ upon field stimulation at 100 Hz, a number which seems not inconsistent with our findings (that is, a reduction by 65%), allowing for the lesser duty cycle of tetanic stimulation compared with continuous depolarization.

As already stated in the companion paper (Sztretye et al., 2011), the measurement of steady $[Ca^{2+}]_{SR}$ agrees well with the average values obtained in mice muscle by Rudolf et al. (2006) using D1ER. In their work, it was found that a single twitch resulted in a variable reduction of R, corresponding to a change in $[Ca^{2+}]_{SR}$ of between 5 and 30% of its resting value. Although these numbers are imprecise and we have not measured depletion during twitches, the decay in $[Ca^{2+}]_{SR}$ that we measure after ~5 ms of depolarization ranged between 5 and 10% of the resting value, in rough agreement with those measurements and also with existing estimates of the amounts of Ca^{2+} that can be released in a twitch (for instance, by Jong et al. [1993]).

The studies by Rudolf et al. (2006) and Canato et al. (2010) with D1ER included a measure of the reduction in R caused by tetanic field stimulation, a reduction which in the first study reached no more than 25% of the initial $R - R_{min}$ value and in the more recent study was of the order of 30% of the initial value (specifically, -0.1 in Fig. 2 of Canato et al. [2010]). All of these estimates of depletion are therefore in rough agreement with the present ones, allowing for the difference in duty cycle of activation.
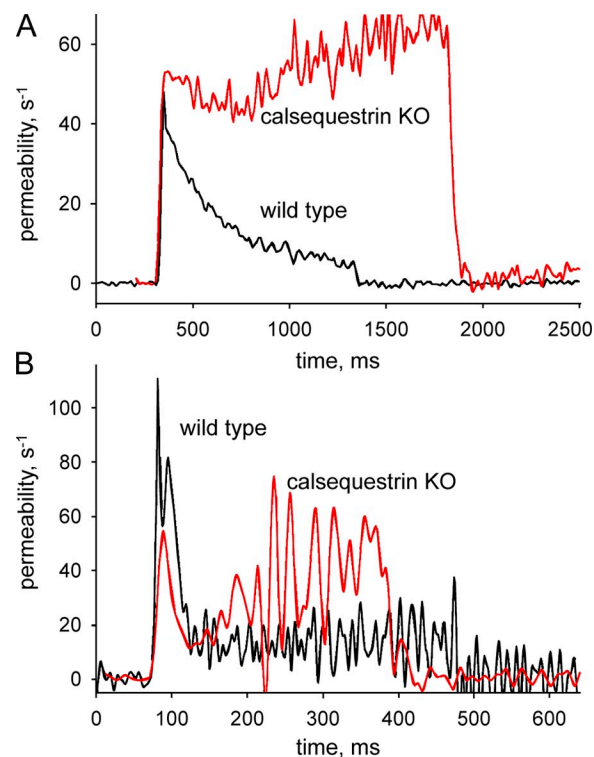

Figure 8. Ca^{2+} release permeability. Permeability, calculated as defined in Eq. 5, during a long-lasting, supramaximal pulse is shown. (A) For cells shown in Figs. 2 and 3, in which the solution in the pipette was EGTA. (B) For cells in Figs. 4 and 5, in which the solution in the pipette was BAPTA. Note how the permeability decays sharply during a pulse in the WT; it either remains elevated or recovers after initially decaying in the Casq KO.

The study of mouse FDB fibers under voltage clamp by Jiménez-Moreno et al. (2010) also showed that R decreased with increasing duration of depolarizations, stabilizing after 150 ms. This decay was again consistent with partial depletion. The magnitude of the decay measured by this group during a long-lasting depolarization averaged only 6% of the available range, whereas it was close to 65% in our case. One possible explanation of the discrepancy is that the sensor was closer to saturation in the earlier paper, and therefore the modest changes in R reflected a disproportionately greater reduction in $[Ca^{2+}]_{SR}$.

Canato et al. (2010) provided a first comparison of the evolution of $[Ca^{2+}]_{SR}$ in WT and Casq1 or Casq1/2-null cells upon physiological activation. They showed that tetanic trains of action potentials caused a much greater depletion in nulls than in WT cells, a result which fully agrees with the present observations under voltage clamp depolarization. The two sets of results demonstrate that these cameleon biosensors can reach close to R_{min} in living cells depleted by depolarization and therefore suggest that the limited decay in R featured in the WT is caused by an actual difference in the evolution of $[Ca^{2+}]_{SR}$ between WT and Casq-null cells.

The four works cited are in qualitative agreement with the present results in showing that prolonged depolarization or tetanic stimulation can only release part of the SR Ca^{2+} content. This is in contrast with the observations of Ziman et al. (2010). Using Fluo-5N loaded preferentially in the SR, these authors found $\sim$90% reduction of $[Ca^{2+}]_{SR}$ in mouse FDB fibers tetanically stimulated at 50 Hz. Although this is by far the greatest depletion reported in any study, it may also be the most reliable measurement, as the work included precise calibrations of the signal in every individual cell. The technique requires loading the buffer BAPTA in AM form, which results in the establishment of a substantial but unknown concentration of active buffer in the cytosol and other compartments of the cells. Although this condition marks a variance with what others have done, our present results suggest that the sole presence of BAPTA in the cytosol does not explain the greater degree of depletion. In any case, Ziman et al. (2010) established that the SR of their WT cells can release more and deplete to a fuller extent than it does in the present experiments. More work is clearly needed to understand the discrepancies.

Casq in the biosensor does not alter Ca^{2+} release

The possible interference by Casq added as part of the biosensor was tested in two ways. Measurements performed with Casq1-fused biosensor were repeated under every condition using Casq with the C-terminal stretch of aspartate residues deleted. This variant was shown to have a greatly reduced ability to bind Ca^{2+} (Shin et al., 2000), a property confirmed by Park et al. (2004),

who also showed that the deletion mutant does not polymerize in aqueous solutions upon Ca^{2+} binding as the native form does. The differences in release flux and degree of depletion between WT and Casq nulls or in the presence of BAPTA were also observed with the deletion variant. However, these properties did not change significantly when measured with one or the other form of the fused biosensor.

In another demonstration of at most modest effects of the extrinsic buffer, we found no visible differences between Ca^{2+} transients and the underlying flux in areas of the same cell expressing the biosensor at different densities. The lack of substantial effects was to be expected, given the concentrations at which the protein was expressed. For example, in the test illustrated by Fig. 7, the concentration of biosensor in the area of high expression was 7.54 µM. Considering that a Casq molecule may provide 60 Ca^{2+} binding sites and that it is probably <50% saturated at rest, the areas of high concentration may have had $\sim$180 µM of additional Ca^{2+}. This is much less than the amount believed to be bound to native Casq, thus justifying the absence of measurable differences in Ca^{2+} release. It is also possible that Casq in fusion with the biosensor cannot engage correctly in the polymerization believed to be needed to attain its high buffering power (Park et al., 2004).

Regulation by lumenal Ca^{2+} has been controversial

Although in the case of cardiac muscle a consensus is emerging regarding the nature of control of Ca^{2+} release channels by lumenal Ca^{2+}, in skeletal muscle the evidence is contradictory. Meissner (1986) showed in SR vesicle preparations that increasing lumenal Ca^{2+} shifts the dependence of flux activation to lower cytosolic $[Ca^{2+}]$. Likewise, Donoso et al. (1995) found that increasing $[Ca^{2+}]_{SR}$ promoted flux from vesicles. Tripathy and Meissner (1996) provided evidence that the promotion was, at least partially, caused by flow-through effects, actions of the increased lumenal Ca^{2+} on the cytosolic regulation sites. Pape et al. (1995, 1998) and Pape and Carrier (1998) described in frog muscle a large increase in release permeability with decreasing SR content, an increase which Pizarro and Ríos (2004) confirmed but evaluated at a much lower value relative to the initial permeability. Interestingly, they also showed that the discrepancy resulted from different estimates of the initial and final values of $[Ca^{2+}]_{SR}$, which neither laboratory could measure at the time. Both groups found evidence to indicate that the increase in permeability with depletion reflects relief from inhibition by Ca^{2+} acting on cytosolic sites. Therefore, none of those works could pin down a truly lumenal regulatory effect of Ca^{2+}.

Also working on frog muscle, Launikonis et al. (2006) studied the effects of changes in $[Ca^{2+}]_{SR}$ (which were measured using shifted excitation and emission ratioing

of Mag-Indo-1) on the properties of Ca^{2+} sparks. Increasing $[Ca^{2+}]_{SR}$ from 250 to 400 µM resulted in a reversible rise in spark frequency by 70%. Although the effect was statistically significant, it was of much lesser magnitude than the increases observed in cardiomyocytes under similar changes of $[Ca^{2+}]_{SR}$.

From this collected evidence, Ríos et al. (2006) concluded that the termination mechanism for skeletal muscle was uncertain. Since that time, evidence has strengthened for a Casq-dependent termination role of $[Ca^{2+}]_{SR}$ in heart cells (most notably with the contribution by Zima et al. [2010]). Two new sets of papers are directly relevant to the role of lumenal Ca^{2+} in skeletal muscle, but they are still contradictory. Qin et al. (2008, 2009) found a clear difference in the behavior of bilayer-reconstituted RyR channels from skeletal and cardiac muscle. Although cardiac channels displayed high sensitivity to $[Ca^{2+}]_{trans}$ (i.e., on the SR lumenal side of the bilayers) when either Casq1 or Casq2 were present (Qin et al., 2008, 2009), skeletal RyR channels did not show such sensitivity (Qin et al., 2009). The observations appeared to rule out a physiological modulation of RyR1 channel gating by Ca^{2+} inside the SR. In contrast, Protasi et al. (2009) and Dainese et al. (2009) demonstrated malignant hyperthermia susceptibility in the Casq1-null mouse and attributed it to a dysregulated RyR1 in the absence of Casq.

Against this backdrop of contradictory findings, the present measurements of permeability, for being direct and reaching repeatable results under varied conditions, strongly support the presence of regulation by lumenal Ca^{2+} mediated by Casq. Canato et al. (2010) added to this picture the observation of similar consequences of the absence of Casq under more physiological stimulation. These results support a dual involvement of store depletion in termination of Ca^{2+} release: a direct reduction of flux as the result of decay in the $[Ca^{2+}]$ gradient and RyR unitary current, plus a mechanism similar to that of cardiac muscle, whereby reduction of $[Ca^{2+}]_{SR}$ below a certain level constitutes a channel-closing signal transduced by Casq.

The present experiments used BAPTA as a tool to hasten release and SR depletion, presumably by inhibiting CDI of the RyRs. There is clear evidence of CDI in frog muscle (Baylor et al., 1983; Melzer et al., 1984; Pape et al., 1995; Pizarro and Ríos, 2004), and the present results support its operation in the mouse. The promotion of release flux by BAPTA demonstrates that CDI is operative in the mouse. Moreover, its observation in both WT and Casq1-null muscles indicates that CDI does not require the presence of Casq. It remains to be tested whether and in what ways Casq, and indirectly $[Ca^{2+}]_{SR}$, modulates the inhibitory effects of cytosolic Ca, changing their extent or time course.

The termination mechanisms in amphibians and mammals

Working on frog skeletal muscle, Shirokova and Ríos (1996) combined long-lasting depolarization under voltage clamp and caffeine applications to demonstrate properties that are strikingly different from those now observed for the mouse. Indeed, the amount of Ca^{2+} releasable by depolarizing pulses was always equal to the amount present in the caffeine-releasable pool. In other words, the depolarization was capable of emptying the SR (or its caffeine-releasable content). Given this property, it was possible to compute a permeability from measured quantities (as the ratio of flux to total Ca^{2+} content in the SR), which was found to increase with progressive depletion of the SR. This essentially direct evaluation of permeability indicates that the Casq-mediated termination mechanism now reported for the mouse is absent in the frog. Fig. 9, combining data from studies by Rengifo et al. (2002) and Royer et al. (2008), clearly demonstrates qualitative differences in the time course of release flux for frogs (green) and mice (black). The much more abrupt decay in the mouse, after the brief shoulder, can now be ascribed to the fall in permeability that operates in the mammal, reflecting an essential difference in the mechanisms that underlie termination of flux in these species. Specifically, the shoulder was described as a stage where flux decays at a rate of order greater than one (Royer et al., 2008). The present study clarifies the reasons for such rapid decay, attributing it both to depletion, which reduces the driving force, and closure of release channels.
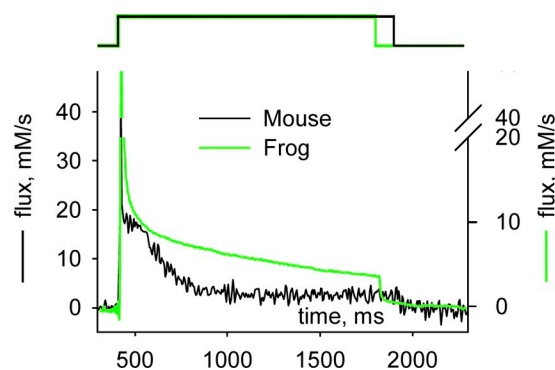

Figure 9. The time course of flux is different in frogs and mice. The black trace shows release flux in a WT mouse FDB cell, activated by the voltage clamp pulse represented at the top. The green trace shows a comparable record for a cell from frog semitendinosus muscle voltage clamped in a Vaseline gap. Records are scaled to match the levels reached after the early peak. Note in the mouse the more complex decay, described as a shoulder. Cells are in similar but not identical solutions designed to block ionic currents. Both internal solutions had 10 mM EGTA. The mouse cell was studied by Royer et al. (2008). The frog cell was studied by Rengifo et al. (2002).

244   A channel-gating role of calsequestrin

SR permeability versus evacuability

A recurrent goal of the studies of Ca^{2+} release is to separate the two mechanisms that determine its evolution, namely, changes in driving force (depletion) and changes in gating, or channel properties. Until the present work, such parsing was hampered because data were limited to Ca^{2+} release flux and its time integral, from which inferences were made about what was left inside the SR. Given those limitations, the traditional approach has been to take as the measure of permeability the depletion-corrected flux (Schneider et al., 1987), defined as

$$\overset{\bullet}{Rel}_C \equiv \frac{\overset{\bullet}{Rel}}{Ca_{SR}},$$

where Ca_{SR} represents total Ca remaining inside the SR. This remainder had to be estimated, which was done assuming that it reaches a low or negligible value after a long depolarization.

Royer et al. (2008, 2010) demonstrated that $\overset{\bullet}{Rel}_C$ is proportional to $\varphi P/B$, where φ is the ratio of SR surface over volume, P is SR Ca^{2+} permeability, and B is SR Ca^{2+} buffering power. Royer et al. (2008) named this product the evacuability, E, and showed that under some circumstances E could be approximated by the normalized flux rate of change, $NFRC$, an index derived from $\overset{\bullet}{Rel}(t)$ (see Supplemental material). Using this approximation, they concluded that E increases during long lasting pulses, as the SR is depleted. Barring shape changes in the SR, an increase in E implies that P increases, B decreases, or that both changes take place.

The present results, specifically the direct measurement of a decreasing P, are difficult to reconcile with an increase in E. We now believe, as argued in the Supplemental material, that E in fact decreases, consistent with the decrease in P. Fig. S2 shows that the error term, separating E from its estimator, $NFRC$, becomes large if some assumptions are not upheld, thus explaining the earlier, wrong conclusion.

Summary

The present two papers demonstrate that the novel tool D4cpv-Casq1 and its variant D4cpv-δAsp provide a calibrated ratiometric measure of $[Ca^{2+}]$ inside the SR of adult mice muscle cells. They yield a measure of stable $[Ca^{2+}]_{SR}$ that on average is not different from earlier estimates and is significantly <1 mM. In agreement with in vitro measurements of the kinetics of the sensor-Ca^{2+} reaction, the changing $[Ca^{2+}]_{SR}$ can be followed dynamically during EC coupling. When this is done in parallel with measurements of $[Ca^{2+}]_c$ and Ca^{2+} release flux, it is revealed that the built-in termination process observed upon depletion of the SR is largely caused by closing of the release channels, which is translated at the cellular level as reduction of the permeability to Ca^{2+} of the SR

membrane. This change requires the presence of Casq because it is absent or strongly modified in Casq1-null mice. It is directly related to the attainment of a set low $[Ca^{2+}]_{SR}$ because it occurs at the same $[Ca^{2+}]_{SR}$ in spite of drastic changes in release kinetics induced by the presence of different Ca^{2+} buffers in the cytosol. Such mechanism is similar to one currently favored to explain the termination of Ca^{2+} sparks of cardiac muscle (e.g., Györke and Terentyev, 2008), which suggests a commonality of devices for control of Ca signals in striated muscles. Finally, the study contributed evidence for CDI of the release channels. In conclusion, $[Ca^{2+}]_c$, $[Ca^{2+}]_{SR}$, and Casq act together to control release termination in mouse muscle.

APPENDIX

$[Ca^{2+}]$ derived kinetically from a ratio signal

The goal of this appendix is to derive the relationship between concentration of a monitored species (represented by C or $[Ca^{2+}]$) and the signal of a ratiometric indicator, sensor, with 1:1 stoichiometry without the usual assumption of instantaneous equilibrium. Such relationship may be considered a kinetic generalization of the Grynkiewicz equation (Grynkiewicz et al., 1985),

$$[Ca^{2+}] = (\beta K_d)\frac{R - R_{min}}{R_{max} - R},$$

which is Eq. 1 in the companion paper (Sztretye et al., 2011) in the case of $n = 1$. Although this derivation uses the language of fluorescence, the expression derived is valid for any property or signal that depends linearly on indicator concentration and changes when the indicator binds to the monitored substance.

Here indicator ratio R is defined as F_2/F_1, where F_1 (also donor) and F_2 (or acceptor) fluorescence satisfies the following:

$$\begin{aligned} F_1 &= (D_T - CD)\varepsilon_1 + CD \times \varepsilon_{1C} \\ F_2 &= (D_T - CD)\varepsilon_2 + CD \times \varepsilon_{2C}. \end{aligned} \tag{A1}$$

D_T is total sensor concentration, CD is concentration of sensor bound to the monitored species, and ε_j is the intensity of fluorescence per micromolar at standard excitation and gain settings. A subindex j equal to 1 or 2 represents, respectively, fluorescence in the donor or acceptor range, with free sensor; j equal to $1C$ or $2C$ represents the corresponding intensity with bound sensor. From Eq. A1 and the definition of R, it follows that

$$CD = \frac{D_T(\varepsilon_2 - R\varepsilon_1)}{R(\varepsilon_{1C} - \varepsilon_1) - (\varepsilon_{2C} - \varepsilon_2)}. \tag{A2}$$

C, the free concentration of the monitored species, satisfies

$$C = \frac{d(CD)/dt + k_{\text{OFF}}CD}{k_{\text{ON}}(D_{\text{T}} - CD)}. \tag{A3}$$

An expression of *C* as a function of *R* is reached by substitution of the value of *CD* from Eq. A2 into Eq. A3:

$$\tag{A4}$$

$$C = \frac{1}{k_{\text{ON}}}\frac{dR}{dt}\frac{\varepsilon_{2C}\varepsilon_1 - \varepsilon_2\varepsilon_{1C}}{[R(\varepsilon_{1C} - \varepsilon_1) - \varepsilon_{2C} + \varepsilon_2](R\varepsilon_{1C} - \varepsilon_{2C})} + K_{\text{d}}\beta\frac{R - R_{\min}}{R_{\max} - R},$$

where $\beta \equiv \varepsilon_1/\varepsilon_{1C}$, $R_{\max} = \varepsilon_{2C}/\varepsilon_{1C}$, and $R_{\min} = \varepsilon_2/\varepsilon_1$.

Eq. A4 can be expressed in terms of indicator ratio by dividing numerator and denominator by $\varepsilon_1\varepsilon_{1C}$

$$C = \frac{\beta}{k_{\text{ON}}}\frac{dR}{dt}\frac{R_{\max} - R_{\min}}{[(R_{\max} - R) + \beta(R - R_{\min})](R_{\max} - R)} + K_{\text{d}}\beta\frac{R - R_{\min}}{R_{\max} - R},$$

which is Eq. 2.

REFERENCES

Baylor, S.M., W.K. Chandler, and M.W. Marshall. 1982. Use of metallochromic dyes to measure changes in myoplasmic calcium during activity in frog skeletal muscle fibres. *J. Physiol.* 331:139–177.

Baylor, S.M., W.K. Chandler, and M.W. Marshall. 1983. Sarcoplasmic reticulum calcium release in frog skeletal muscle fibres estimated from Arsenazo III calcium transients. *J. Physiol.* 344:625–666.

Canato, M., M. Scorzeto, M. Giacomello, F. Protasi, C. Reggiani, and G.J. Stienen. 2010. Massive alterations of sarcoplasmic reticulum free calcium in skeletal muscle fibers lacking calsequestrin revealed by a genetically encoded probe. *Proc. Natl. Acad. Sci. USA.* 107:22326–22331. doi:10.1073/pnas.1009168108

Dainese, M., M. Quarta, A.D. Lyfenko, C. Paolini, M. Canato, C. Reggiani, R.T. Dirksen, and F. Protasi. 2009. Anesthetic- and heat-induced sudden death in calsequestrin-1-knockout mice. *FASEB J.* 23:1710–1720. doi:10.1096/fj.08-121335

Donoso, P., H. Prieto, and C. Hidalgo. 1995. Luminal calcium regulates calcium release in triads isolated from frog and rabbit skeletal muscle. *Biophys. J.* 68:507–515. doi:10.1016/S0006-3495(95)80212-2

Eisenberg, B.R. 1983. Quantitative ultrastructure of muscle. *In* Handbook of Physiology: Skeletal Muscle. L.D. Peachey, editor. Lippincott Williams and Wilkins. 73–112.

Escobar, A.L., P. Velez, A.M. Kim, F. Cifuentes, M. Fill, and J.L. Vergara. 1997. Kinetic properties of DM-nitrophen and calcium indicators: rapid transient response to flash photolysis. *Pflugers Arch.* 434:615–631. doi:10.1007/s004240050444

Grynkiewicz, G., M. Poenie, and R.Y. Tsien. 1985. A new generation of Ca2+ indicators with greatly improved fluorescence properties. *J. Biol. Chem.* 260:3440–3450.

Györke, S., and D. Terentyev. 2008. Modulation of ryanodine receptor by luminal calcium and accessory proteins in health and cardiac disease. *Cardiovasc. Res.* 77:245–255. doi:10.1093/cvr/cvm038

Györke, S., S.C. Stevens, and D. Terentyev. 2009. Cardiac calsequestrin: quest inside the SR. *J. Physiol.* 587:3091–3094. doi:10.1113/jphysiol.2009.172049

Jiménez-Moreno, R., Z.M. Wang, M.L. Messi, and O. Delbono. 2010. Sarcoplasmic reticulum Ca^{2+} depletion in adult skeletal muscle fibres measured with the biosensor D1ER. *Pflugers Arch.* 459:725–735. doi:10.1007/s00424-009-0778-4

Jong, D.S., P.C. Pape, W.K. Chandler, and S.M. Baylor. 1993. Reduction of calcium inactivation of sarcoplasmic reticulum calcium release by fura-2 in voltage-clamped cut twitch fibers from frog muscle. *J. Gen. Physiol.* 102:333–370. doi:10.1085/jgp.102.2.333

Kabbara, A.A., and D.G. Allen. 2001. The use of the indicator fluo-5N to measure sarcoplasmic reticulum calcium in single muscle fibres of the cane toad. *J. Physiol.* 534:87–97. doi:10.1111/j.1469-7793.2001.00087.x

Launikonis, B.S., J. Zhou, L. Royer, T.R. Shannon, G. Brum, and E. Ríos. 2006. Depletion "skraps" and dynamic buffering inside the cellular calcium store. *Proc. Natl. Acad. Sci. USA.* 103:2982–2987. doi:10.1073/pnas.0511252103

Meissner, G. 1986. Ryanodine activation and inhibition of the Ca^{2+} release channel of sarcoplasmic reticulum. *J. Biol. Chem.* 261:6300–6306.

Melzer, W., E. Ríos, and M.F. Schneider. 1984. Time course of calcium release and removal in skeletal muscle fibers. *Biophys. J.* 45:637–641. doi:10.1016/S0006-3495(84)84203-4

Melzer, W., E. Ríos, and M.F. Schneider. 1987. A general procedure for determining the rate of calcium release from the sarcoplasmic reticulum in skeletal muscle fibers. *Biophys. J.* 51:849–863. doi:10.1016/S0006-3495(87)83413-6

Palmer, A.E., C. Jin, J.C. Reed, and R.Y. Tsien. 2004. Bcl-2-mediated alterations in endoplasmic reticulum Ca2+ analyzed with an improved genetically encoded fluorescent sensor. *Proc. Natl. Acad. Sci. USA.* 101:17404–17409. doi:10.1073/pnas.0408030101

Palmer, A.E., M. Giacomello, T. Kortemme, S.A. Hires, V. Lev-Ram, D. Baker, and R.Y. Tsien. 2006. Ca2+ indicators based on computationally redesigned calmodulin-peptide pairs. *Chem. Biol.* 13:521–530. doi:10.1016/j.chembiol.2006.03.007

Paolini, C., M. Quarta, A. Nori, S. Boncompagni, M. Canato, P. Volpe, P.D. Allen, C. Reggiani, and F. Protasi. 2007. Reorganized stores and impaired calcium handling in skeletal muscle of mice lacking calsequestrin-1. *J. Physiol.* 583:767–784. doi:10.1113/jphysiol.2007.138024

Pape, P.C., and N. Carrier. 1998. Effect of sarcoplasmic reticulum (SR) calcium content on SR calcium release elicited by small voltage-clamp depolarizations in frog cut skeletal muscle fibers equilibrated with 20 mM EGTA. *J. Gen. Physiol.* 112:161–179. doi:10.1085/jgp.112.2.161

Pape, P.C., D.S. Jong, and W.K. Chandler. 1995. Calcium release and its voltage dependence in frog cut muscle fibers equilibrated with 20 mM EGTA. *J. Gen. Physiol.* 106:259–336. doi:10.1085/jgp.106.2.259

Pape, P.C., D.S. Jong, and W.K. Chandler. 1998. Effects of partial sarcoplasmic reticulum calcium depletion on calcium release in frog cut muscle fibers equilibrated with 20 mM EGTA. *J. Gen. Physiol.* 112:263–295. doi:10.1085/jgp.112.3.263

Park, H., I.Y. Park, E. Kim, B. Youn, K. Fields, A.K. Dunker, and C. Kang. 2004. Comparing skeletal and cardiac calsequestrin structures and their calcium binding: a proposed mechanism for coupled calcium binding and protein polymerization. *J. Biol. Chem.* 279:18026–18033. doi:10.1074/jbc.M311553200

Pizarro, G., and E. Ríos. 2004. How source content determines intracellular Ca^{2+} release kinetics. Simultaneous measurement of $[Ca^{2+}]$ transients and $[H^+]$ displacement in skeletal muscle. *J. Gen. Physiol.* 124:239–258. doi:10.1085/jgp.200409071

Protasi, F., C. Paolini, and M. Dainese. 2009. Calsequestrin-1: a new candidate gene for malignant hyperthermia and exertional/environmental heat stroke. *J. Physiol.* 587:3095–3100. doi:10.1113/jphysiol.2009.171967

Qin, J., G. Valle, A. Nani, A. Nori, N. Rizzi, S.G. Priori, P. Volpe, and M. Fill. 2008. Luminal Ca^{2+} regulation of single cardiac ryanodine receptors: insights provided by calsequestrin and its mutants. *J. Gen. Physiol.* 131:325–334. doi:10.1085/jgp.200709907

Qin, J., G. Valle, A. Nani, H. Chen, J. Ramos-Franco, A. Nori, P. Volpe, and M. Fill. 2009. Ryanodine receptor luminal Ca2+ regulation: swapping calsequestrin and channel isoforms. *Biophys. J.* 97:1961–1970. doi:10.1016/j.bpj.2009.07.030

Rengifo, J., R. Rosales, A. González, H. Cheng, M.D. Stern, and E. Ríos. 2002. Intracellular Ca(2+) release as irreversible Markov process. *Biophys. J.* 83:2511–2521. doi:10.1016/S0006-3495(02)75262-4

Ríos, E., B.S. Launikonis, L. Royer, G. Brum, and J. Zhou. 2006. The elusive role of store depletion in the control of intracellular calcium release. *J. Muscle Res. Cell Motil.* 27:337–350. doi:10.1007/s10974-006-9082-5

Royer, L., S. Pouvreau, and E. Ríos. 2008. Evolution and modulation of intracellular calcium release during long-lasting, depleting depolarization in mouse muscle. *J. Physiol.* 586:4609–4629. doi:10.1113/jphysiol.2008.157990

Royer, L., M. Sztretye, C. Manno, S. Pouvreau, J. Zhou, B.C. Knollmann, F. Protasi, P.D. Allen, and E. Ríos. 2010. Paradoxical buffering of calcium by calsequestrin demonstrated for the calcium store of skeletal muscle. *J. Gen. Physiol.* 136:325–338. doi:10.1085/jgp.201010454

Rudolf, R., P.J. Magalhães, and T. Pozzan. 2006. Direct in vivo monitoring of sarcoplasmic reticulum Ca2+ and cytosolic cAMP dynamics in mouse skeletal muscle. *J. Cell Biol.* 173:187–193. doi:10.1083/jcb.200601160

Schneider, M.F., B.J. Simon, and G. Szucs. 1987. Depletion of calcium from the sarcoplasmic reticulum during calcium release in frog skeletal muscle. *J. Physiol.* 392:167–192.

Schuhmeier, R.P., and W. Melzer. 2004. Voltage-dependent Ca^{2+} fluxes in skeletal myotubes determined using a removal model analysis. *J. Gen. Physiol.* 123:33–51. doi:10.1085/jgp.200308908

Schuhmeier, R.P., E. Gouadon, D. Ursu, N. Kasielke, B.E. Flucher, M. Grabner, and W. Melzer. 2005. Functional interaction of CaV channel isoforms with ryanodine receptors studied in dysgenic myotubes. *Biophys. J.* 88:1765–1777. doi:10.1529/biophysj.104.051318

Shin, D.W., J. Ma, and D.H. Kim. 2000. The asp-rich region at the carboxyl-terminus of calsequestrin binds to $Ca(^{2+})$ and interacts with triadin. *FEBS Lett.* 486:178–182. doi:10.1016/S0014-5793(00)02246-8

Shirokova, N., and E. Ríos. 1996. Activation of Ca2+ release by caffeine and voltage in frog skeletal muscle. *J. Physiol.* 493:317–339.

Sztretye, M., J. Yi, L. Figueroa, J. Zhou, L. Royer, P.D. Allen, and E. Ríos. 2011. D4cpv-calsequestrin: a sensitive ratiometric biosensor accurately targeted to the calcium store of skeletal muscle. *J. Gen. Physiol.* 138:211–229. doi:10.1085/jgp.201010591

Tripathy, A., and G. Meissner. 1996. Sarcoplasmic reticulum lumenal Ca^{2+} has access to cytosolic activation and inactivation sites of skeletal muscle Ca2+ release channel. *Biophys. J.* 70:2600–2615. doi:10.1016/S0006-3495(96)79831-4

Ursu, D., R.P. Schuhmeier, and W. Melzer. 2005. Voltage-controlled Ca2+ release and entry flux in isolated adult muscle fibres of the mouse. *J. Physiol.* 562:347–365. doi:10.1113/jphysiol.2004.073882

Wetzel, P., and G. Gros. 1998. Decay of Ca2+ and force transients in fast- and slow-twitch skeletal muscles from the rat, mouse and Etruscan shrew. *J. Exp. Biol.* 201:375–384.

Wu, Y.C., T. Tucker, and R. Fettiplace. 1996. A theoretical study of calcium microdomains in turtle hair cells. *Biophys. J.* 71:2256–2275. doi:10.1016/S0006-3495(96)79429-8

Zima, A.V., E. Bovo, D.M. Bers, and L.A. Blatter. 2010. Ca^{2+} spark-dependent and -independent sarcoplasmic reticulum Ca^{2+} leak in normal and failing rabbit ventricular myocytes. *J. Physiol.* 588:4743–4757. doi:10.1113/jphysiol.2010.197913

Ziman, A.P., C.W. Ward, G.G. Rodney, W.J. Lederer, and R.J. Bloch. 2010. Quantitative measurement of $Ca^2(^+)$ in the sarcoplasmic reticulum lumen of mammalian skeletal muscle. *Biophys. J.* 99:2705–2714. doi:10.1016/j.bpj.2010.08.032